Nanoscale

ROYAL SOCIETY OF CHEMISTRY

COMMUNICATION

View Article Online
View Journal | View Issue

Check for updates

Cite this: *Nanoscale*, 2020, **12**, 5359

Received 28th January 2020,
Accepted 11th February 2020

DOI: 10.1039/d0nr00752h

rsc.li/nanoscale

Hierarchical CuO@ZnCo LDH heterostructured nanowire arrays toward enhanced water oxidation electrocatalysis†

Ting Wang,[a] Xiaoxue Zhang,[a] Xiaojuan Zhu,[a] Qian Liu,[b] Siyu Lu,[c] Abdullah M. Asiri,[d] Yonglan Luo*[a] and Xuping Sun*[b]

It is of great importance to design and develop complex heterostructured nanocatalysts with superior electrochemical performance to that of single structured ones. Here, we report the hydrothermal fabrication of a hierarchical heterostructured CuO@ZnCo layered double hydroxide nanowire array on a copper foil (CuO@ZnCo LDH/CF). As a self-supported electrocatalyst for water oxidation, CuO@ZnCo LDH/CF has superior catalytic activity with the requirement of a low overpotential of 270 mV to attain 10 mA cm^{-2} in 1.0 M KOH. In addition, it shows strong durability to maintain its activity for at least 24 h.

Recently, considerable efforts have been devoted to explore alternative energy storage and conversion systems due to the increased global energy demand and environmental concerns caused by fossil fuel combustion.[1,2] Hydrogen is an ideal candidate with the advantages of high energy output and carbon-free combustion products, and electrochemical water splitting offers an attractive route to produce highly pure hydrogen.[3–6] Water electrolysis involves a cathodic hydrogen evolution reaction (HER) and an anodic oxygen evolution reaction (OER).[7] However, the anodic water oxidation reaction is rather energy intensive with a minimal initiation potential of 1.23 V *vs.* reversible hydrogen electrode (RHE); this remains the critical limitation in the improvement of water splitting technologies, and efficient water oxidation catalysts (WOCs) must be used to drive high current densities at low overpotentials.[8–10] As the benchmark WOCs, RuO_2 and IrO_2 suffer from scarcity and high cost.[11,12] As such, there is a great need to design and develop efficient WOCs made of earth-abundant elements.

Co has emerged as an interesting transition metal due to its catalytic power toward electrochemical water oxidation.[6,8,13–23] Layered double hydroxides (LDHs) consist of cationic metal hydroxide layers and exchangeable interlayer anions,[24] which have been intensively studied as attractive WOCs in basic solutions.[25–28] As a typical bimetallic LDH, ZnCo LDH is also promising for water oxidation electrocatalysis.[29–31] Constructing a 3D hierarchical structure on a conductive substrate is an effective strategy to promote ultimate catalytic activity owing to the exposure of more active sites and the facilitated diffusion of the electrolyte and gas.[32–34] However, to the best of our knowledge, a ZnCo LDH-based architecture as a high-performance WOC has not been reported before.

In this study, we describe the development of a CuO@ZnCo-LDH core–shell heterostructured nanowire array on a copper foil (CuO@ZnCo LDH/CF) as an efficient electrocatalyst for OER in alkaline media. CuO@ZnCo LDH/CF only requires an overpotential of 270 mV to achieve 10 mA cm^{-2} in 1.0 M KOH, which is 110 mV less than that for ZnCo LDH/CF. Notably, this 3D catalyst electrode also demonstrates excellent long-term electrochemical durability.

CuO@ZnCo LDH/CF was prepared by hydrothermally growing ZnCo LDH on a CuO nanowire array supported on CF (CuO NW/CF). Fig. S1a† shows the X-ray diffraction (XRD) pattern of CuO NW/CF with peaks at 35.5° and 38.9° assigned to the (002) and (200) planes of monoclinic CuO (JCPDS no. 05-0661), respectively. Three other strong peaks at 43.3°, 50.4° and 74.1° are ascribed to CF (JCPDS no. 85-1326). After the hydrothermal reaction, the XRD pattern of CuO@ZnCo LDH/CF (Fig. 1a) shows several new diffraction peaks assigned to a typical ZnCo LDH.[35] Fig. S1b† and Fig. 1(b and c) show the SEM images of CuO NW/CF and CuO@ZnCo LDH/CF, respectively. It is clear that the smooth surface of CuO NW is uniformly covered with dense ZnCo LDH, indicating the typical

---

[a] *Chemical Synthesis and Pollution Control Key Laboratory of Sichuan Province, School of Chemistry and Chemical engineering, China West Normal University, Nanchong 637002, Sichuan, China. E-mail: luoylcwnu@hotmail.com*
[b] *Institute of Fundamental and Frontier Sciences, University of Electronic Science and Technology of China, Chengdu 610054, Sichuan, China. E-mail: xpsun@uestc.edu.cn*
[c] *Green Catalysis Center and College of Chemistry, Zhengzhou University, Zhengzhou 450001, Henan, China*
[d] *Chemistry Department, Faculty of Science & Center of Excellence for Advanced Materials Research, King Abdulaziz University, P.O. Box 80203, Jeddah 21589, Saudi Arabia*

† Electronic supplementary information (ESI) available: Experimental section and supplementary figures. See DOI: 10.1039/d0nr00752h

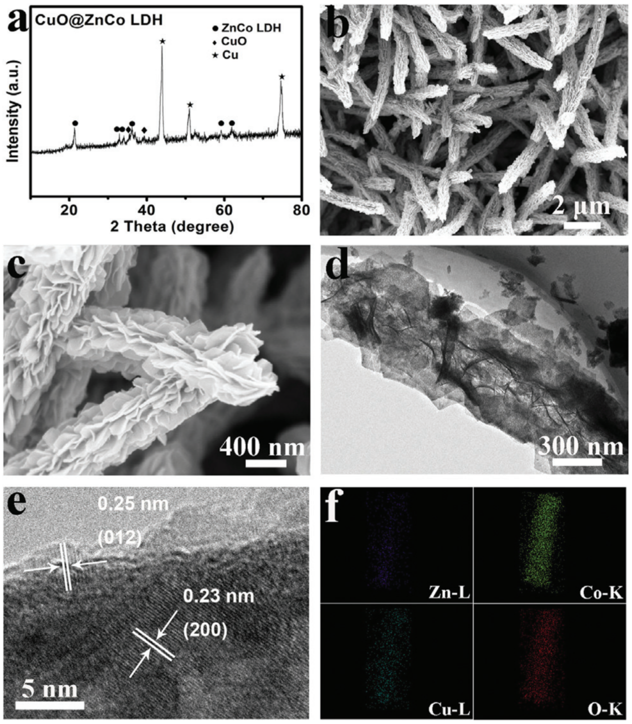

Fig. 1 (a) XRD pattern of CuO@ZnCo LDH/CF. (b and c) SEM images of CuO@ZnCo LDH/CF. (d and e) TEM and HRTEM images of a CuO@ZnCo LDH nanowire. (f) EDX elemental mapping images of Zn, Co, Cu, and O for CuO@ZnCo LDH.

core–shell structure of CuO@ZnCo LDH. This can be further confirmed by the transmission electron microscopy (TEM) image of a CuO@ZnCo LDH nanowire (Fig. 1d). From the high-resolution TEM (HRTEM) image of CuO@ZnCo LDH (Fig. 1e), lattice fringes can be observed, and the interplanar spacings are measured to be 0.23 and 0.25 nm, corresponding to the (200) plane of CuO and the (012) plane of LDH. Meanwhile, most of the lattice fringes overlap and cross, indicating that the ZnCo LDH shell has a heterogeneous overlapping spatial structure and constituent distribution, which is also the cause of the weak diffraction peaks in the XRD pattern of ZnCo LDH.[38] Moreover, the corresponding energy-dispersive X-ray (EDX) elemental mapping images of CuO@ZnCo LDH confirm the uniform distribution of the Zn, Co, Cu, and O elements (Fig. 1f). The EDX spectrum (Fig. S2†) reveals that the atomic ratio of Zn, Co, Cu, and O is approximately 6.55 : 19.72 : 10.23 : 63.50.

Fig. 2a shows the X-ray photoelectron spectra (XPS) of CuO@ZnCo LDH. In the Zn 2p region, the two Zn 2p$_{1/2}$ and Zn 2p$_{3/2}$ peaks are located at the binding energies (BEs) of 1021.8 and 1045 eV, respectively; this is in good agreement with the reported data of the Zn 2p states in ZnCo LDH.[36] The Co 2p$_{1/2}$ region shows two peaks at 797.5 and 796.2 eV, while the Co 2p$_{3/2}$ region shows two other peaks at 781.5 and 780.2 eV (Fig. 2b), indicating the presence of the Co^{3+} and Co^{2+} oxidation states.[37,38] In the Cu 2p region (Fig. 2c), the two peaks at 933.9 and 953.9 eV can be assigned to Cu 2p$_{3/2}$ and Cu 2p$_{1/2}$, respectively, with satellites (identified as "Sat.") at 941.5, 943.9 and 962.4 eV, which are in accordance with the typical characteristics of Cu^{2+} in CuO.[39] The two peaks at 529.7 and 531.5 eV in the O 1s region can be attributed to O^{2-} and OH^{-}, respectively.[39] All the above-mentioned results suggest the successful formation of CuO@ZnCo LDH/CF.

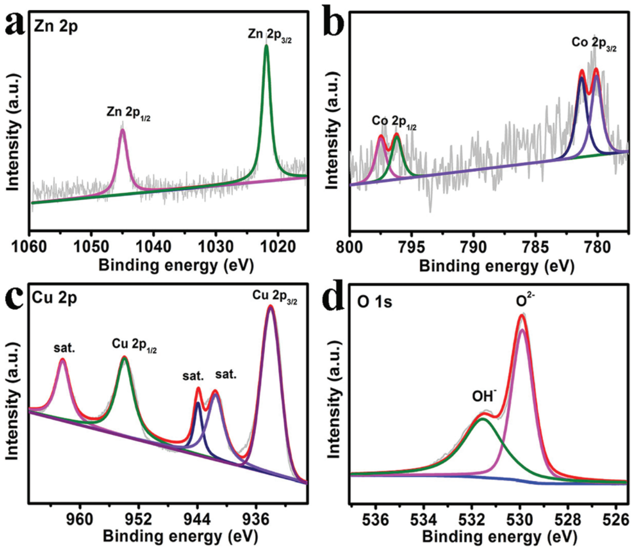

Fig. 2 XPS spectra of CuO@ZnCo LDH in the (a) Zn 2p, (b) Co 2p, (c) Cu 2p, and (d) O 1s regions.

CuO@ZnCo LDH/CF (CuO@ZnCo LDH mass loading: 10 mg cm^{-2}) was directly used as a 3D working electrode for OER catalysis in 1.0 M KOH in a typical three-electrode setup with a scan rate of 2 mV s^{-1}. For comparison, ZnCo LDH/CF, CuO NW/CF, CF, and RuO$_2$/CF with the same loading were also examined under the same conditions. Because the measured reaction currents cannot directly reflect the intrinsic behavior of catalysts due to the effect of ohmic resistance, an *iR* correction was applied for all initial data for further analysis.[40] Fig. 3a shows the linear sweep voltammetry (LSV) curves on the reversible hydrogen electrode (RHE) scale. RuO$_2$ is highly active, while bare CF has poor catalytic activity for OER. CuO NW/CF and ZnCo LDH/CF were active to catalyze OER but needed large overpotentials of 398 and 380 mV to drive 10 mA cm^{-2}, respectively. It is worth mentioning that CuO@ZnCo LDH/CF showed much superior catalytic activity to that of ZnCo LDH/CF. CuO@ZnCo LDH/CF only needed an overpotential as low as 270 mV at 10 mA cm^{-2}, which was 110 mV less than that for ZnCo LDH/CF. This overpotential also compared favorably to the behaviors of most reported Co-based OER catalysts in alkaline media (Table S1†). Fig. 3b presents the corresponding Tafel plots. The Tafel slope of CuO@ZnCo LDH/CF was 100 mV dec^{-1}, and it was much lower than that for ZnCo LDH/CF (128 mV dec^{-1}), CuO@ NRs/CF (145 mV dec^{-1}), and CF (214 mV dec^{-1}), implying faster OER kinetics on CuO@ZnCo LDH/CF. Fig. 3c exhibits the multistep chronopotentiometric curve for CuO@ZnCo LDH/CF with the current ranging from 10 to 120 mA cm^{-2} (20 mA cm^{-2} per 500

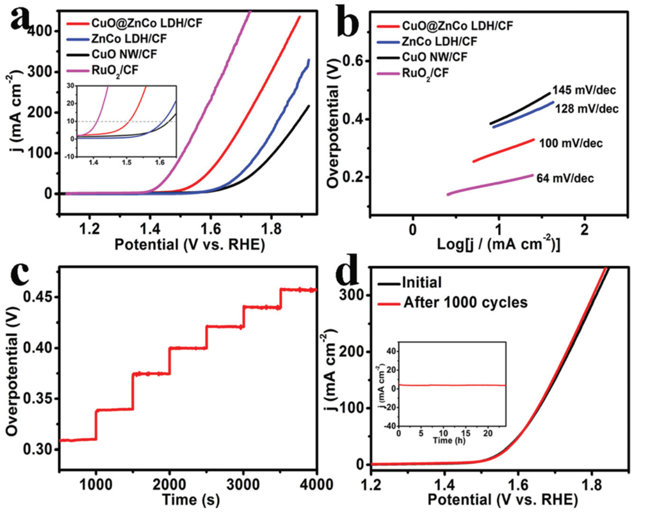

Fig. 3 (a) Polarization curves of CF, CuO NW/CF, ZnCo LDH/CF, CuO@ZnCo LDH/CF, and RuO_2/CF for OER with a scan rate of 2 mV s^{-1}. (b) Tafel plots of CF, CuO NW/CF, ZnCo LDH/CF, CuO@ZnCo LDH/CF, and RuO_2/CF. (c) Chronopotentiometric curve obtained for CuO@ZnCo LDH/CF at multi-current-step from 10 to 120 mA cm^{-2}. (d) LSV curves for CuO@ZnCo LDH/CF before and after 1000 CV cycles (inset: time-dependent current density curve at a fixed overpotential of 270 mV). All experiments were carried out in 1.0 M KOH.

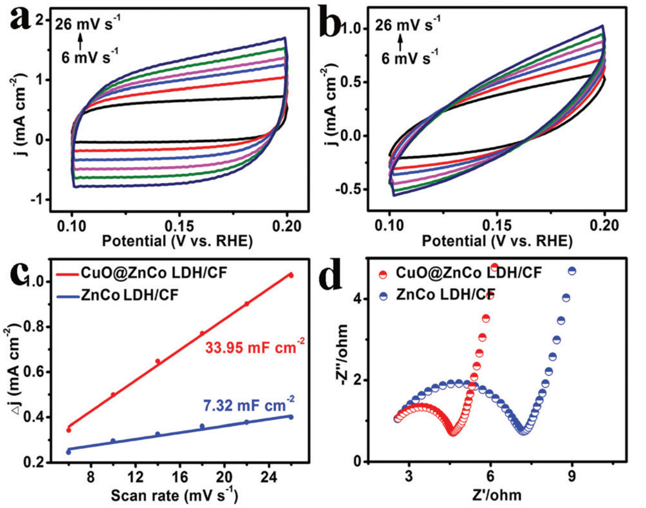

Fig. 4 CVs of CuO@ZnCo LDH/CF (a) and ZnCo LDH/CF (b) in the non-faradaic capacitance current range at the scan rates of 6, 10, 14, 18, 22, and 26 mV s^{-1}. (c) Capacitive currents at 0.15 V *vs.* Hg/HgO as a function of scan rate for CuO@ZnCo LDH/CF and ZnCo LDH/CF. (d) Nyquist plots of CuO@ZnCo LDH/CF electrode and ZnCo LDH/CF electrode.

s). The potential immediately leveled off at 1.53 V at the initial current value and remained unchanged for 500 s; others also showed similar results, indicating the outstanding conductivity, mechanical robustness, and mass transportation of the CuO@ZnCo LDH/CF electrode.[41,42] We also probed the durability of CuO@ZnCo LDH/CF. As shown in Fig. 3d, after continuous cyclic voltammetry (CV) scanning for 1000 cycles in 1.0 M KOH, the obtained LSV curve shows a negligible difference in current densities compared with the initial one. The SEM (Fig. S3†), TEM (Fig. S4†) and XPS (Fig. S5†) data also suggested almost no changes after the stability test for the catalyst. The inset in Fig. 3d presents the time-dependent current density curve at a fixed overpotential of 270 mV, suggesting that this electrode retains its catalytic activity for at least 24 h. In addition, after the stability tests, the obtained LSV curve shows a negligible difference in the current densities compared with the initial one (Fig. S6†).

We measured the double-layer capacitance (C_{dl}) at the solid–liquid interface of CuO@ZnCo LDH/CF and ZnCo LDH/CF to estimate their electrochemically active surface area (ECSA). Fig. 4a and b show the cyclic voltammograms (CVs) recorded in the region from 0.1 V to 0.2 V *vs.* Hg/HgO. It is suggested that CuO@ZnCo LDH/CF has a much higher C_{dl} value of 33.95 mF cm^{-2} than ZnCo LDH/CF (7.32 mF cm^{-2}), as shown in Fig. 4c; this indicates that CuO@ZnCo LDH/CF as a hierarchical 3D nanoarray electrode has a larger electrochemically active surface area with more exposed active sites for water oxidation electrocatalysis.[43] Electrochemical impedance spectroscopy analysis (Fig. 4d) demonstrated that CuO@ZnCo LDH/CF has a much smaller radius of the semicircle and thus lower charge transfer resistance compared to ZnCo LDH/CF, indicating a higher charge transfer rate and more rapid electrode kinetics for CuO@ZnCo LDH/CF.[44,45]

In summary, CuO@ZnCo LDH/CF has been successfully proven as an efficient and stable 3D catalyst electrode for water oxidation in alkaline conditions. CuO@ZnCo LDH/CF showed greatly enhanced catalytic activity and only needed an overpotential of 270 mV to deliver 10 mA cm^{-2} in 1.0 M KOH, which was 110 mV less compared to that for ZnCo LDH/CF. The superior activity can be ascribed to the increased electrochemically active surface area and electron transfer. This study would open new opportunities in designing and developing other LDH-based hierarchical heterostructured nanoarrays for applications toward water oxidation electrocatalysis.

Conflicts of interest

There are no conflicts to declare.

References

1 N. S. Lewis and D. G. Nocera, *Proc. Natl. Acad. Sci. U. S. A.*, 2006, **103**, 15729–15735.
2 M. Graetzel, *Acc. Chem. Res.*, 1981, **14**, 376–384.
3 T. Feng, Q. Zeng, S. Lu, M. Yang, S. Tao, Y. Chen, Y. Zhao and B. Yang, *ACS Sustainable Chem. Eng.*, 2019, **7**, 7047–7057.
4 R. F. Service, *Science*, 2009, **324**, 1257–1259.
5 W. Li, Y. Liu, M. Wu, X. Feng, S. A. T. Redfern, Y. Shang, X. Yong, T. Feng, K. Wu, Z. Liu, B. Li, Z. Chen, J. S. Tse, S. Lu and B. Yang, *Adv. Mater.*, 2018, **30**, 1800676.

6 D. Wu, Y. Wei, X. Ren, X. Ji, Y. Liu, X. Guo, Z. Liu, A. M. Asiri, Q. Wei and X. Sun, *Adv. Mater.*, 2018, **30**, 1705366.

7 C. Guo, Y. Jiao, Y. Zheng, J. Luo, K. Davey and S. Qiao, *Chem*, 2019, **5**, 2429–2441.

8 J. Wang, W. Cui, Q. Liu, Z. Xing, A. M. Asiri and X. Sun, *Adv. Mater.*, 2016, **28**, 215–230.

9 T. Ma, S. Dai, M. Jaroniec and S. Qiao, *Angew. Chem., Int. Ed.*, 2014, **53**, 7281–7285.

10 W. Zhu, R. Zhang, F. Qu, A. M. Asiri and X. Sun, *ChemCatChem*, 2017, **9**, 1721–1743.

11 Y. Lee, J. Suntivich, K. J. May, E. E. Perry and Y. Shao-Horn, *J. Phys. Chem. Lett.*, 2012, **3**, 399–404.

12 J. Liu, Y. Zheng, Z. Wang, Z. Lu, A. Vasileff and S. Qiao, *Chem. Commun.*, 2018, **54**, 463–466.

13 Y. Wei, X. Ren, H. Ma, X. Sun, Y. Zhang, X. Kuang, T. Yan, H. Ju, D. Wu and Q. Wei, *Chem. Commun.*, 2018, **54**, 1533–1536.

14 T. Liu, L. Xie, J. Yang, R. Kong, G. Du, A. M. Asiri, X. Sun and L. Chen, *ChemElectroChem*, 2017, **4**, 1840–1845.

15 B. S. Yeo and A. T. Bell, *J. Am. Chem. Soc.*, 2011, **133**, 5587–5593.

16 D. Zhou, L. He, R. Zhang, S. Hao, X. Hou, Z. Liu, G. Du, A. M. Asiri, C. Zheng and X. Sun, *Chem. – Eur. J.*, 2017, **23**, 15601–15606.

17 T. Ma, S. Dai, M. Jaroniec and S. Qiao, *J. Am. Chem. Soc.*, 2014, **136**, 13925–13931.

18 Y. Zhu, T. Ma, M. Jaroniec and S. Qiao, *Angew. Chem., Int. Ed.*, 2017, **56**, 1324–1328.

19 W. Lu, T. Liu, L. Xie, C. Tang, D. Liu, S. Hao, F. Qu, G. Du, Y. Ma, A. M. Asiri and X. Sun, *Small*, 2017, **13**, 1700805.

20 Y. Zhang, B. Ouyang, J. Xu, G. Jia, S. Chen, R. S. Rawat and H. J. Fan, *Angew. Chem., Int. Ed.*, 2016, **55**, 8670–8674.

21 D. González-Flores, I. Sánchez, I. Zaharieva, K. Klingan, J. Heidkamp, P. Chernev, P. W. Menezes, M. Driess, H. Dau and M. L. Montero, *Angew. Chem., Int. Ed.*, 2015, **54**, 2472–2476.

22 L. Yang, D. Liu, S. Hao, R. Kong, A. M. Asiri, C. Zhang and X. Sun, *J. Mater. Chem. A*, 2017, **5**, 7305–7308.

23 S. Zhang, B. Ni, H. Li, H. Lin, H. Zhu, H. Wang and X. Wang, *Chem. Commun.*, 2017, **53**, 8010–8013.

24 Q. Wang and D. O'Hare, *Chem. Rev.*, 2012, **112**, 4124–4155.

25 X. Long, J. Li, S. Xiao, K. Yan, Z. Wang, H. Chen and S. Yang, *Angew. Chem., Int. Ed.*, 2014, **53**, 7584–7588.

26 H. Liang, F. Meng, M. Cabán-Acevedo, L. Li, A. Forticaux, L. Xiu, Z. Wang and S. Jin, *Nano Lett.*, 2015, **15**, 1421–1427.

27 F. Song and X. Hu, *J. Am. Chem. Soc.*, 2014, **136**, 16481–16484.

28 Z. Cai, X. Bu, P. Wang, J. C. Ho, J. Yang and X. Wang, *J. Mater. Chem. A*, 2014, **2**, 13250–13258.

29 X. Zou, A. Goswami and T. Asefa, *J. Am. Chem. Soc.*, 2019, **7**, 5069–5089.

30 Y. Li, L. Zhang, X. Xiang, D. Yan and F. Li, *J. Mater. Chem. A*, 2014, **2**, 13250–13258.

31 C. Qiao, Y. Zhang, Y. Zhu, C. Cao, X. Bao and J. Xu, *J. Mater. Chem. A*, 2015, **3**, 6878–6883.

32 T. Liu, D. Liu, F. Qu, D. Wang, L. Zhang, R. Ge, S. Hao, Y. Ma, G. Du, A. M. Asiri, L. Chen and X. Sun, *Adv. Energy Mater.*, 2017, **7**, 1700020.

33 L. Xie, F. Qu, Z. Liu, X. Ren, S. Hao, R. Ge, G. Du, A. M. Asiri, X. Sun and L. Chen, *J. Mater. Chem. A*, 2017, **5**, 7806–7810.

34 J. Shan, Y. Zheng, B. Shi, K. Davey and S. Qiao, *ACS Energy Lett.*, 2019, **4**, 2719–2730.

35 X. Zou, A. Goswami and T. Asefa, *J. Am. Chem. Soc.*, 2013, **135**, 17242–17245.

36 M. Shao, F. Ning, M. Wei, D. G. Evans and X. Duan, *Adv. Funct. Mater.*, 2014, **24**, 580–586.

37 X. Xiang, L. Zhang, H. I. Hima, F. Li and D. G. Evans, *Appl. Clay Sci.*, 2009, **42**, 405–409.

38 S. Zhang, H. Zhu and Y. Zheng, *Electrochim. Acta*, 2019, **299**, 281–288.

39 G. Liu, X. He, D. He, B. Cui, L. Zhu, H. Suo and C. Zhao, *J. Mater. Sci.: Mater. Electron.*, 2019, **30**, 2080–2088.

40 R. Zhang, Z. Wang, R. Ge, X. Ren, S. Hao, F. Qu, Z. Liu, G. Du, A. M. Asiri, B. Zheng and X. Sun, *ACS Sustainable Chem. Eng.*, 2017, **5**, 8518–8522.

41 X. Ren, W. Wang, R. Ge, S. Hao, F. Qu, G. Du, A. M. Asiri, Q. Wei, L. Chen and X. Sun, *Chem. Commun.*, 2017, **53**, 9000–9003.

42 D. Liu, T. Liu, L. Zhang, F. Qu, G. Du, A. M. Asiri and X. Sun, *J. Mater. Chem. A*, 2017, **5**, 3208–3213.

43 Q. Liu, L. Xie, Z. Liu, G. Du, A. M. Asiri and X. Sun, *Chem. Commun.*, 2017, **53**, 12446–12449.

44 C. Guo, L. Zhang, J. Miao, J. Zhang and C. M. Li, *Adv. Energy Mater.*, 2013, **3**, 167–171.

45 X. Xiong, Y. Ji, M. Xie, C. You, L. Yang, Z. Liu, A. M. Asiri and X. Sun, *Electrochem. Commun.*, 2018, **86**, 161–165.